ACS Catalysis

Research Article

pubs.acs.org/acscatalysis

Bifunctional Rhodium Cocatalysts for Photocatalytic Steam Reforming of Methane over Alkaline Titanate

Katsuya Shimura,[†] Hiromasa Kawai,[†] Tomoko Yoshida,[‡] and Hisao Yoshida*[,†]

[†]Department of Applied Chemistry, Graduate School of Engineering, and [‡]Division of Integrated Research Projects, EcoTopia Science Institute, Nagoya University, Nagoya 464-8603, Japan

Supporting Information

ABSTRACT: Photocatalytic steam reforming of methane (PSRM; 2 H_2O (g) + CH_4 → 4 H_2 + CO_2) was examined over metal-loaded $K_2Ti_6O_{13}$ photocatalysts. Although the production rate was improved by loading Pt cocatalyst on the $K_2Ti_6O_{13}$ photocatalyst, unfavorable formation of CO and gradual deactivation of photocatalyst were observed. On the other hand, a Rh-loaded $K_2Ti_6O_{13}$ sample showed two times higher activity than the Pt-loaded one did, and promoted the PSRM selectively without deactivation for many hours. In the highly active Rh-loaded photocatalyst, the Rh cocatalyst existed as a mixture of small metallic rhodium and large rhodium oxide particles. The photocatalytic activity tests for hydrogen evolution and oxygen evolution from each aqueous solution of sacrificial reagent (methanol and silver nitrate, respectively) revealed that the metallic rhodium particles and the rhodium oxide particles could function as cocatalysts preferably for reduction and oxidation, respectively. Also on a $Na_2Ti_6O_{13}$ photocatalyst, a mixture of rhodium metal and oxide similarly enhanced the photocatalytic activity. Thus, it is suggested that the Rh cocatalyst on these alkaline titanates bifunctionally promoted the PSRM.

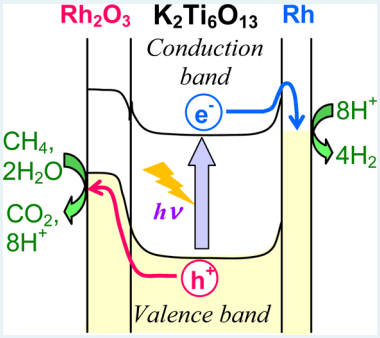

KEYWORDS: *photocatalytic steam reforming of methane, hydrogen, alkaline titanate, bifunctional rhodium cocatalyst, Rh K-edge XAFS*

1. INTRODUCTION

Development of a hydrogen production method from renewable resources and natural energy is important for the realization of a sustainable society. Biomethane is one of the possible hydrogen sources.[1] Our research group found that some kinds of Pt-loaded semiconductors, such as Pt/TiO_2, Pt/$NaTaO_3$:La, Pt/Ga_2O_3, and Pt/$CaTiO_3$, promoted photocatalytic steam reforming of methane (PSRM; CH_4 + 2H_2O → 4H_2 + CO_2) around room temperature.[2−9] The PSRM using biomethane can be considered as a sustainable technology for conversion of solar energy into the storable chemical potential of hydrogen. The current efficiency of this photocatalytic system is, however, still far from practical use, and thus the development of more efficient photocatalyst is desired.

Loading cocatalysts is one of the effective ways to improve the photocatalytic activity, and various cocatalysts have been developed by many researchers. For example, NiO_x,[10−12] RuO_2,[13] and Rh−Cr[14,15] cocatalysts are effective for increasing the activity of various photocatalysts in water decomposition. PdS,[16] MoS_2,[17] and NiS[18] cocatalysts can increase the photocatalytic activity of CdS photocatalyst in hydrogen production from water. Ru[19] and Pt−Ru[20] cocatalysts can improve the oxynitride photocatalysts for hydrogen production from aqueous alcohol solution. Pt[21] and Pd[22] cocatalysts can enhance the activity of WO_3 photocatalyst in the degradation of organic compounds. Of course, Pt-loaded TiO_2 photocatalysts have been very famous for exhibiting high photocatalytic activities in various reactions.[1,23−29]

Alkaline titanates such as potassium titanate ($K_2Ti_6O_{13}$) can function as photocatalysts, for example, the $K_2Ti_6O_{13}$ photocatalysts with RuO_2 and Pt cocatalysts were reported to be active for water splitting.[30,31] Since the activation of water would be one of the important steps in the PSRM, we had expected that the alkaline titanates could be active for the PSRM. Recently, we found that a Rh-loaded $K_2Ti_6O_{13}$ photocatalyst showed a high activity for the PSRM, and the hydrogen production rate over this sample was higher than that over a Pt-loaded $K_2Ti_6O_{13}$ photocatalyst and reported as a rapid communication.[32] In the present study, effective cocatalysts were investigated for the PSRM on alkaline titanate photocatalysts, mainly on a $K_2Ti_6O_{13}$ photocatalyst. We examined the influence of the loading method on both the structure of the Rh cocatalyst and their activity for the PSRM. An efficient bifunctional Rh-cocatalyst for the alkaline titanate photocatalysts is proposed here.

2. EXPERIMENTAL METHODS

2.1. Preparation of Photocatalysts. A $K_2Ti_6O_{13}$ photocatalyst was prepared by a solid-state reaction method. Starting materials, K_2CO_3 (Kishida, 99.5%) and rutile-TiO_2 (Kojundo, 99.9%), were mechanically mixed in a stoichiometric ratio by a wet ball-milling method: alumina balls (150 g, 1 cm in

Received: November 29, 2011
Revised: September 6, 2012
Published: September 6, 2012

   dx.doi.org/10.1021/cs2006229 | ACS Catal. 2012, 2, 2126−2134

diameter), starting materials (ca. 20 g), and acetone (80 mL) were put into a capped plastic bottle (300 mL), mixed at 120 rpm for 24 h at room temperature, and dried in an oven at 333 K overnight. The mixed powder was calcined in air atmosphere at 1273 K for 10 h in a platinum crucible. After cooling it to room temperature, it was ground by an alumina mortar and washed with distilled water. A $Na_2Ti_6O_{13}$ sample was prepared by the same procedure as the $K_2Ti_6O_{13}$ sample, where Na_2CO_3 (Kishida, 99.5%) was used instead of K_2CO_3 as the starting material.

TiO_2 and β-Ga_2O_3 samples were also used for comparison. The TiO_2 sample (JRC-TIO-8, anatase, 338 m^2 g^{-1}) was supplied from the Catalysis Society of Japan and calcined in air atmosphere at 673 K for 6 h before use. The β-Ga_2O_3 sample was commercially obtained (Kojundo, 99.99%) and used as received.

The powdery semiconductor photocatalysts were loaded with metal cocatalysts (Rh, Pt, Ru, Pd, and Au). The loading amount (x) of these metals was in the range from 0.01 to 1 wt %. The employed precursors were as follows; $RhCl_3{\cdot}3H_2O$ (Kishida, 99%), $H_2PtCl_6{\cdot}6H_2O$ (Wako, 99.9%), $(NH_4)_3RuCl_6$ (Mitsuwa, chemical grade), $PdCl_2$ (Kishida, 99%) and $HAuCl_4$ (Kishida, 99%). Cocatalysts were loaded by an impregnation method or an oxidative photodeposition method. In the impregnation method, the photocatalyst powder (2.0 g) was dispersed into an aqueous solution (50 mL) of the metal precursor and stirred for 0.5 h, followed by evaporation to dryness with a rotary evaporator. Then, the dried powder was calcined in air atmosphere at 773 K for 2 h, and/or reduced in a flow of hydrogen (10 mL min^{-1}) at 473 K for 0.5 h. In the photodeposition method, the photocatalyst (2.5 g) was dispersed into an aqueous methanol solution (10%, 400 mL) containing precursor of metal cocatalyst in a beaker with vigorous stirring, followed by photoirradiation from above by using a 300 W xenon lamp, which entirely emitted from UV to visible light, for 2 h with continuous stirring. In the present condition, the solution would contain a certain amount of dissolved oxygen from the atmosphere (the oxidative photodeposition method). Then, the photocatalyst was separated by suction filtration, washed with distilled water, and dried at 323 K. By way of comparison, another Rh-loaded $K_2Ti_6O_3$ sample was prepared by an in situ photodeposition method in the absence of oxygen,[3] that is, the $K_2Ti_6O_3$ adsorbing the rhodium precursor in the solution was separated and dried, followed by successive photoirradiation in a quartz cell for the photocatalytic reaction (60 × 20 × 1 mm^3) in a flow of water vapor and methane with argon. The sample with the cocatalyst (x wt %) was referred to as Rh(x)/$K_2Ti_6O_{13}$ for example.

2.2. Photocatalytic Reaction Tests. The reaction tests were carried out with a fixed-bed flow reactor.[3] The photocatalyst was granulated to the size of 400−600 μm. The quartz cell was filled with a mixture of the photocatalyst (0.8 g) and quartz granules (0−0.6 g). The reaction gas, a mixture of water vapor and methane with argon, was introduced into the reactor at the flow rate of 40 mL min^{-1} and the reaction started upon photoirradiation with the 300 W xenon lamp. In a standard condition, the concentration of water vapor and methane was 1.5% and 50%, respectively, and the light of the entire wavelength region from the xenon lamp was irradiated without passing any filters, where the light intensity measured in the range of 254 ± 10 and 365 ± 15 nm were 14 and 60 mW cm^{-2}, respectively. The temperature of the reaction cell became 323 K during the photoirradiation. The products were analyzed by an online gas chromatograph with a thermal conductivity detector to detect H_2, CO_2, and CO. Hydrogen production rates shown in figures and tables were the values at 6 h after the reaction started unless otherwise stated.

Test reactions for hydrogen evolution from an aqueous methanol solution and oxygen evolution from an aqueous solution of silver nitrate were carried out. The photocatalyst (0.4 g) was dispersed into an aqueous solution (10 mL) of methanol (20 vol%) or silver nitrate (0.01 mol/L) in a cylindrical quartz reactor with vigorous stirring. After the gas phase was purged by argon gas, the light of the entire wavelength region from the xenon lamp was irradiated from the bottom (16 cm^2) of the reactor under a flow of argon. The outlet gas was analyzed similarly by the online gas chromatography.

2.3. Characterizations of Photocatalysts. Powder X-ray diffraction (XRD) pattern was recorded at room temperature on a Rigaku diffractometer MiniFlexII/AP using Ni-filtered Cu Kα radiation (30 kV, 15 mA). The mean crystallite size of the $K_2Ti_6O_{13}$ sample was estimated from the diffraction line at 30.3 degree with the Scherrer equation. Diffuse reflectance (DR) UV−visible spectrum was recorded at room temperature on a JASCO V-570 equipped with an integrating sphere covered with $BaSO_4$, where $BaSO_4$ was used as the reference. The Brunauer−Emmett−Teller (BET) specific surface area was calculated from the amount of N_2 adsorption at 77 K, which was measured by a Quantachrome Monosorb. Scanning electron microscopy (SEM) images were recorded by a S-5200 (Hitachi). Transmission electron microscopy (TEM) images were recorded by a JEOL electron microscope (JEM-2100M, 200 kV) equipped with CCD camera (Gatan, erlangshen ES500W). Rh K-edge XAFS (X-ray Absorption Fine Structure) were recorded at the NW-10A[33] station of KEK-PF (Photon Factory, Institute of Materials Structure Science, High Energy Accelerator Research Organization, Japan) at room temperature with a Si(311) double crystal monochromator in a transmission mode for a rhodium foil, and in a fluorescence mode by using the Lytle-detector[34] (100 mm ion chamber filled with krypton) with a ruthenium filter (μt = 6) for the Rh-loaded samples. The spectra were analyzed with a REX 2000 software (Rigaku). Fourier transform of Rh K-edge EXAFS was performed in the range of about 3−12 $Å^{-1}$. The inverse Fourier transform was carried out in the range of about 0.9−3.2 Å, and the curve fitting analysis was performed by using theoretical parameters.[35]

3. RESULTS AND DISCUSSION

3.1. Effect of Cocatalyst. The prepared $K_2Ti_6O_{13}$ sample was characterized. From the XRD pattern, it was assignable to $K_2Ti_6O_{13}$ (ICSD #25712) and no impurity phase was observed (Figure 1A). The mean crystallite size of the sample was 22 nm. From the DR UV−vis spectrum, absorption assigned to TiO_2 (rutile) was not observed (Figure 1B). The bandgap estimated from the absorption edge was about 3.4 eV. BET specific surface area of the sample was 2.3 m^2 g^{-1}. From the SEM image, the sizes of aggregated particles were within the range from 0.1 to 2 μm (Figure 1C).

Figure 2 shows the time courses of the production rates over the Pt(0.085)/$K_2Ti_6O_{13}$ sample. Production of both hydrogen and carbon dioxide was observed, and the initial production rates were high. However, the production rates gradually decreased with time, and a small amount of carbon monoxide was produced constantly as a minor byproduct (Figure 2c).

dx.doi.org/10.1021/cs2006229 | ACS Catal. 2012, 2, 2126−2134

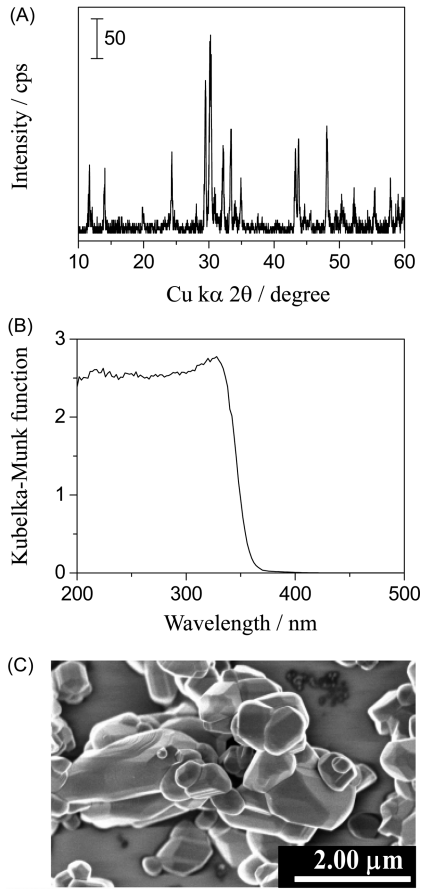

Figure 1. (A) XRD pattern, (B) DR UV–vis spectrum, and (c) SEM image of the $K_2Ti_6O_{13}$ sample.

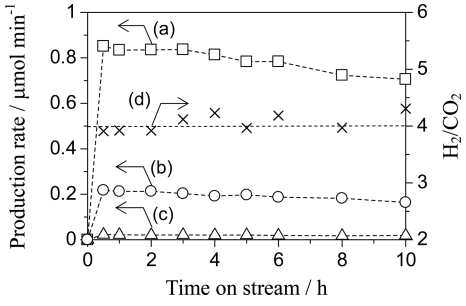

Figure 2. Time course of the production rate of (a) H_2, (b) CO_2, and (c) CO on the Pt(0.085)/$K_2Ti_6O_{13}$ sample, and (d) that of molar ratio of the produced H_2 and CO_2 (H_2/CO_2) in the flowing mixture of water vapor and methane. The Pt cocatalyst was loaded by the photodeposition method.

The molar ratio of hydrogen and carbon dioxide (Figure 2d) was almost four at first but became slightly higher than four. According to the previous studies, it is suggested that the deactivation would be due to surface accumulation of byproduct,[3] or structural changes of the Pt cocatalyst.[4]

On the other hand, the Rh-loaded $K_2Ti_6O_{13}$ photocatalyst showed a high and stable activity although an induction period for the production rate was observed (Figure 3). The induction period might be due to an accumulation of the reaction intermediates as suggested in the previous studies,[3−5] or an additional reduction of the Rh cocatalyst might occur in the induction period upon the photoirradiation in the flow of water vapor and methane as the Rh cocatalyst was partially oxidized

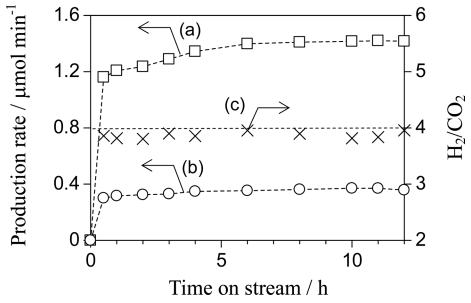

Figure 3. Time course of the production rate of (a) H_2 and (b) CO_2 on the Rh(0.04)/$K_2Ti_6O_{13}$ sample, and (c) that of molar ratio of the produced H_2 and CO_2 (H_2/CO_2) in the flowing mixture of water vapor and methane. The Rh cocatalyst was loaded by the photodeposition method.

as mentioned later. After the induction period, the production rate was constant, and the molar ratio of hydrogen to carbon dioxide was almost four. No formation of byproduct such as carbon monoxide was observed. These results show that the PSRM would selectively proceed on the Rh/$K_2Ti_6O_{13}$ photocatalyst.

Figure 4 shows the hydrogen production rate at 6 h after the reaction started in the flow of water vapor and methane over

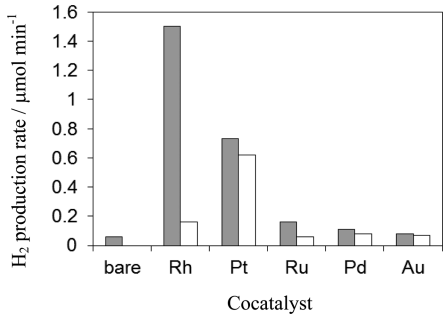

Figure 4. Hydrogen production rate over the bare $K_2Ti_6O_{13}$ sample and the metal(0.03)-loaded $K_2Ti_6O_{13}$ samples prepared by the photodeposition method (filled column) and the impregnation method followed by calcination at 773 K (open column).

the bare $K_2Ti_6O_{13}$ sample, the various metal(0.03 wt %)-loaded $K_2Ti_6O_{13}$ samples prepared by the photodeposition method and the samples prepared by the impregnation method followed by calcination at 773 K. As often reported for TiO_2 photocatalyst,[3,36] the sample prepared by the photodeposition method exhibited higher activity than the sample prepared by the impregnation and successive calcination. The hydrogen production rates over the Ru-, Pd-, and Au-loaded samples were slightly higher than, or almost the same as, that over the bare $K_2Ti_6O_{13}$ sample. On the other hand, loading Rh or Pt cocatalyst largely improved the activity. It is noted that the highest activity among them was obtained over the Rh/$K_2Ti_6O_{13}$ photocatalyst prepared by the photodeposition method.

Figure 5 shows the influence of the Rh- and Pt-loading amount on the photocatalytic activity. With increasing the loading amount, the activity of the Rh-loaded samples increased and then decreased: the highest production rate was obtained with the 0.03 wt %-loaded sample (Figure 5a). On the other hand, the Pt-loaded samples showed similar activities to each other (Figure 5b). The hydrogen production rate over the best

dx.doi.org/10.1021/cs2006229 | ACS Catal. 2012, 2, 2126–2134

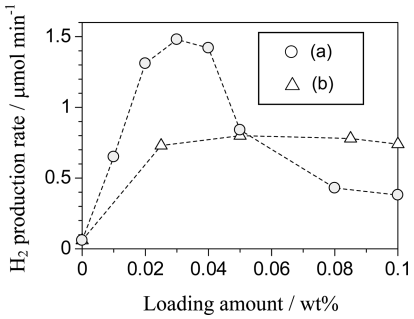

Figure 5. Influence of the loading amount of (a) Rh and (b) Pt cocatalysts on the hydrogen production rate in the flowing mixture of water vapor and methane. The Rh and Pt cocatalysts were loaded on the $K_2Ti_6O_{13}$ sample by the photodeposition method.

$Rh/K_2Ti_6O_{13}$ photocatalyst was two times higher than those of the present Pt-loaded samples.

The best $Rh/K_2Ti_6O_{13}$ photocatalyst exhibited higher activity than those over the reported Pt/TiO_2,[3] Pt/Ga_2O_3,[5] and $Pt/CaTiO_3$[6] photocatalysts, and similar activity to that over the $Pt/NaTaO_3$:La photocatalyst[4] under the same reaction condition. No clear correlation was observed between the specific surface areas of these samples and their photocatalytic activities for the PSRM. As reported in the previous studies,[2−8] several factors such as the crystal defects, the specific surface area, and the crystal structure of the semiconductor would influence the activity for the PSRM.

A reverse reaction of the PSRM, photocatalytic reaction between hydrogen and carbon dioxide, was examined over the bare $K_2Ti_6O_{13}$ sample and the 0.03 wt % metal (Rh, Pt, Ru, Pd or Au)-loaded $K_2Ti_6O_{13}$ samples in the flow of the reaction mixture (H_2 5% and CO_2 12.5% with an argon balance, 40 mL min^{-1}). All these samples did not form any products such as CO and CH_4 in the present condition, that is, no reverse reaction occurred. Thus, it is revealed that each cocatalyst would contribute only to the forward reaction of the PSRM.

3.2. Influence of Rh-loading Method. Figure 6 shows the photocatalytic activities of the following five samples: three

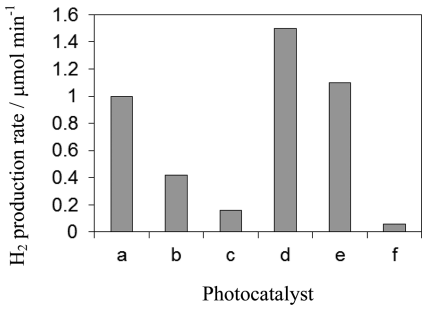

Figure 6. Hydrogen production rate in the PSRM over (a)−(e) the $Rh(0.03)/K_2Ti_6O_{13}$ samples and (f) the bare $K_2Ti_6O_{13}$ sample. The Rh cocatalyst was loaded by (a−c) the impregnation method and successive thermal pretreatments, (d) the oxidative photodeposition method, and (e) the in situ photodeposition method. For the thermal treatment condition, see the text.

$Rh(0.03)/K_2Ti_6O_{13}$ samples were prepared by impregnation and successive different thermal treatments, that is, (a) reduction at 473 K, (b) calcination at 773 K before reduction at 473 K, and (c) calcination at 773 K. Another sample (d) was prepared by the photodeposition method in the presence of dissolved oxygen (the oxidative photodeposition). The other sample (e) was prepared by the in situ photodeposition method in an anaerobic condition. Among these five samples, the catalyst prepared by the oxidative photodeposition method (Figure 6d) showed the highest activity. Among the samples prepared by the impregnation method, the reduced sample (Figure 6a) showed the highest activity. The sample reduced after calcination (Figure 6b) showed a higher activity than the calcined sample (Figure 6c). Between the two samples prepared by photodeposition, the sample prepared in an aerobic condition (Figure 6d) showed higher activity that that prepared in an anaerobic condition (Figure 6e). Thus, it is proposed that the presence of dissolved oxygen during the photodeposition would provide highly active cocatalyst.

To discuss the local structure of the Rh cocatalysts, XAFS studies of four $Rh(0.1)/K_2Ti_6O_{13}$ samples were carried out. To obtain clear spectra, the Rh contents of these samples were slightly increased compared to the samples for the photocatalytic reaction tests (Figure 6). The Rh K-edge XANES and their derivative spectra (Figure 7A and 7B) revealed that the Rh cocatalyst would be almost metallic on the samples prepared both by the impregnation and successive reduction method (referred to as sample *a*) and by the impregnation, calcination, and reduction method (sample *b*). On the other hand, large

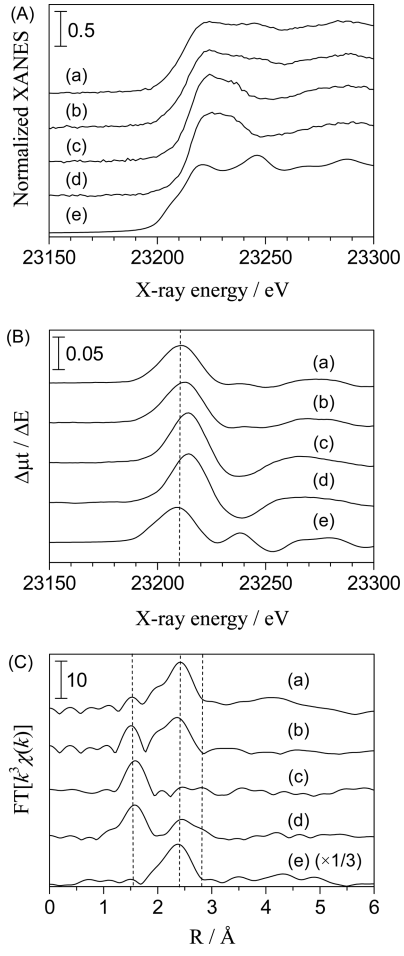

Figure 7. (A) Rh K-edge XANES, (B) derivative spectra of the XANES, and (C) Fourier transforms of Rh K-edge EXAFS for (a−d) the $Rh(0.1)/K_2Ti_6O_{13}$ samples (the samples *a*−*d* in the text) and (e) rhodium foil.

dx.doi.org/10.1021/cs2006229 | *ACS Catal.* 2012, 2, 2126−2134

edge shifts to higher energy suggested that the Rh cocatalyst would be almost oxidized on the samples prepared both by the impregnation and calcination method (sample *c*) and by the oxidative photodeposition method (sample *d*).

Figure 7C shows the Fourier transforms of their Rh K-edge EXAFS. The curve-fitting analysis clarified that the peaks observed at 1.6 and 2.8 Å were assignable to the Rh−O and Rh−Rh shells in rhodium oxide, respectively. The atomic distance of the Rh−O shell was 2.06 Å, which is close to the Rh−O distance in Rh_2O_3 (2.03−2.05 Å, ICSD #108941) but different from that in RhO_2 (1.93−2.02 Å, ICSD #28498). The curve-fitting analysis also provided that the peak observed at 2.4 Å was assignable to the Rh−Rh shell with atomic distance of 2.70 Å, which is consistent with the Rh−Rh distance in rhodium metal (2.69 Å, ICSD #650218). For the sample *a*, a very small peak and a large peak were observed at 1.6 and 2.4 Å, respectively, although the intensity of the latter peak (the Rh−Rh shell) was not so large as compared with that for the rhodium foil. These results indicate that the Rh species on the sample *a* would dominantly exist as relatively large metal nanoparticles. For the sample *b*, two peaks at 1.6 and 2.4 Å were observed, suggesting that both small metal and oxide moieties would coexist on it. For the sample *c*, a large peak at 1.6 Å and a small peak at 2.8 Å were observed, while the peak at 2.4 Å was hardly observed, showing that the Rh species would mainly exist as relatively large oxide particles. For the sample *d*, a clear peak at 1.6 Å, a relatively small peak at 2.4 Å, and a shoulder at 2.8 Å were observed, showing that there were small metal and large oxide moieties.

The TEM images of the samples prepared by the impregnation method (samples *a*−*c*) showed small particles less than 10 nm in diameter, as representatively shown in Figures 8 a−c. Many spherical particles were observed for the samples *a* and *b*, while relatively asymmetric particles were observed for the sample *c*. On the other hand, for the sample *d*, not only the small spherical particles less than 10 nm but also asymmetric particles as large as 50 nm were observed (Figures 8 d and e).

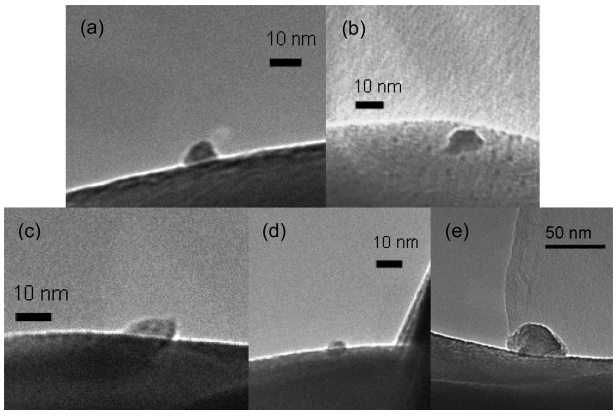

Figure 8. TEM images of the $Rh(0.1)/K_2Ti_6O_{13}$ samples; the sample *a* (a), the sample *b* (b), the sample *c* (c), and the sample *d* (d and e). As for the samples *a*−*d*, see the text.

Combined with the results of EXAFS analysis, it is suggested that the smaller spherical particles (typically around 10 nm in diameter) in the TEM images would be rhodium metal nanoparticles, while the larger asymmetric ones (such as a few dozen nanometers) would be rhodium oxide particles. The Rh species on the sample *a* would be metallic nanoparticles. For the sample *b*, considering the sequential thermal treatment, the nanoparticles would consist of the oxide core and the metallic shell although a part of them might be totally metallic. On the sample *c*, they should be entirely oxidized nanoparticles. On the sample *d* the Rh species would be a mixture of small metallic nanoparticles and large oxide nanoparticles. Thus, it is proposed that the high photocatalytic activity of the sample *d* would originate from the coexistence of the two kinds of nanoparticles, that is, the metallic and oxide nanoparticles.

3.3. Proposed Mechanism. In general, it is considered that precious metal cocatalysts should accept the photoexcited electrons from the conduction band of the semiconductor and function as the reduction sites in the photocatalytic reaction. On the other hand, the some metal oxides such as RuO_2[37−39] and IrO_2[40−42] are proposed or confirmed to work as the oxidation sites. As for the rhodium oxide cocatalyst, Harriman et al. reported that Rh_2O_3 worked as a catalyst for oxygen evolution under photoelectrochemical condition with a photosensitizer and a sacrificial reagent ($Na_2S_2O_8$),[43] and Hrussanova et al. found that a RhO_x electrode in an acid solution exhibited an activity for the electrochemical oxygen evolution.[44] Thus, rhodium oxide can be expected to function as the oxidation sites in the photocatalytic reactions.

To confirm the function of the rhodium metal and oxide cocatalysts, two test reactions were examined: the hydrogen production from an aqueous solution of methanol and the oxygen evolution from an aqueous solution of silver nitrate over the bare $K_2Ti_6O_{13}$ and the samples *a*, *c*, and *d* (Table 1). Since methanol and silver cation are known as efficient electron donor and acceptor, respectively, these reactions are often employed as the test reactions to check the reductive and oxidative activities of photocatalysts, respectively. For the sample *c* on which the rhodium oxide nanoparticles were loaded, the oxygen evolution rate was clearly (more than two times) higher than the bare sample, while the hydrogen production rate was not largely improved (Table 1, entry 3). This indicates that the rhodium oxide cocatalyst preferably promotes the oxidative reaction. The sample *a* with the rhodium metal cocatalyst exhibited much higher activity for the hydrogen production (six times higher than the bare sample), but lower activity for the oxygen production than the sample *c* did (Table 1, entry 2). This indicates that the rhodium metal cocatalyst preferably promotes the reductive reaction. The sample *d*, on which both rhodium metal and oxide nanoparticles were deposited independently, provided the highest activities for both the hydrogen production and the oxygen

Table 1. Photocatalytic Production Rates of Hydrogen from an Aqueous Solution of Methanol and Oxygen from That of Silver Nitrate over the $K_2Ti_6O_{13}$ Sample and the $Rh(0.1)/K_2Ti_6O_{13}$ Samples (the Samples *a*, *c*, and *d*)[a]

		production rate/μmol min^{-1}	
entry	photocatalyst	hydrogen[b]	oxygen[c]
1	$K_2Ti_6O_{13}$	0.13	0.032
2	sample *a*	0.81	0.066
3	sample *c*	0.27	0.080
4	sample *d*	0.88	0.079

[a]For the samples *a*, *c*, and *d*, see the text. [b]Hydrogen production rate from an aqueous methanol solution. [c]Oxygen production rate from an aqueous solution of silver nitrate.

dx.doi.org/10.1021/cs2006229 | ACS Catal. 2012, 2, 2126−2134

production (Table 1, entry 4), suggesting that both the rhodium metal and the oxide nanoparticles can accelerate the reduction and oxidation, respectively. These results support that, in the PSRM, the rhodium metal and oxide nanoparticles on the sample *d* would simultaneously promote the reductive production of hydrogen and the oxidative production of carbon dioxide, respectively, and the cooperative promotion would provide the high photocatalytic performance.

Rhodium oxide (Rh_2O_3) is a *p*-type semiconductor. The bandgap and the electron affinity of the bulk Rh_2O_3 crystal are reported to be 1.4 and 3.6 eV, respectively (Figure 9Aa),[45]

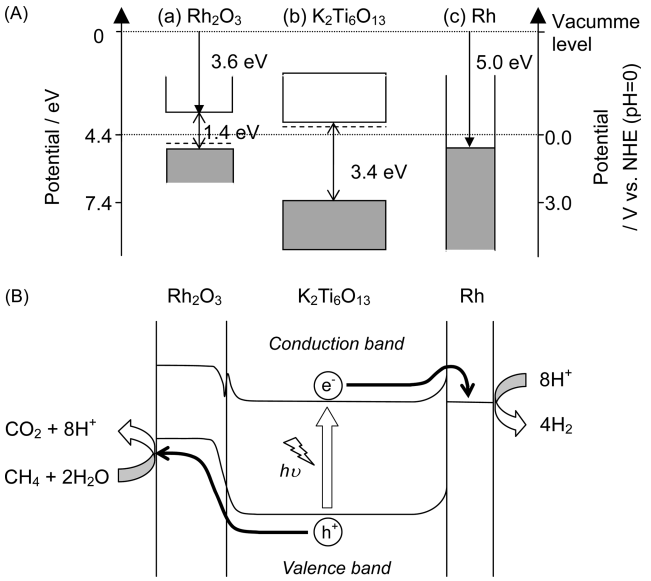

Figure 9. (A) Band structure of (a) Rh_2O_3, (b) $K_2Ti_6O_{13}$, and (c) rhodium metal, and (B) proposed mechanism in the PSRM over the $Rh/Rh_2O_3/K_2Ti_6O_{13}$ prepared by the photodeposition method.

which means the potential of the valence band edge in the bulk crystal of Rh_2O_3 is 0.6 V vs NHE (at pH = 0) and does not satisfy the oxidative potential of water (1.23 V vs NHE at pH = 0). However, as mentioned, the rhodium oxide nanoparticles (a few dozen nanometers) on the $K_2Ti_6O_{13}$ photocatalyst actually promoted the oxygen evolution (Table 1, entry 3), suggesting that the valence band edge of the nanosized rhodium oxide cocatalyst had positive potential enough for the oxidation of water. On the other hand, $K_2Ti_6O_{13}$ is an *n*-type semiconductor, the bandgap of which is 3.4 eV (Figure 1B). It was reported that for metal oxide without partly filled d-levels, the potential of the valence band edge was generally around 2.94 V (vs NHE).[46] Thus, the band structure of $K_2Ti_6O_{13}$ can be estimated as shown in Figure 9Ab. The work function of the bulk crystal of rhodium metal was reported to be 5.0 eV (Figure 9Ac).[47] Since the sizes of the rhodium metal particles on the $K_2Ti_6O_{13}$ sample were as small as 10 nm, the Fermi level of the rhodium metal would positively shift to some extent, which was calculated to be about 0.05 eV (vs NHE) according to the equation reported in the literature.[48] The junction between the rhodium metal and the $K_2Ti_6O_{13}$ semiconductor would change both the Fermi level and the band potentials with generation of the Schottky barrier, and the junction between the Rh_2O_3 particles (*p*-type semiconductor) and the $K_2Ti_6O_{13}$ (*n*-type semiconductor) would change their potentials to form smooth band bending between their valence bands as shown in Figure 9B.

From the above, we propose the photocatalytic reaction mechanism over the $Rh/Rh_2O_3/K_2Ti_6O_{13}$ photocatalyst prepared by the present oxidative photodeposition method as follows: The small rhodium metal particles less than 10 nm would enhance the hydrogen production and promote the separation of the photoexcited electrons from the conduction band of the $K_2Ti_6O_{13}$ photocatalyst. On the other hand, the rhodium oxide particles with a few dozen nanometers would accelerate the oxidation of methane into carbon dioxide ($CH_4 + 2\ H_2O + 8\ h^+ \rightarrow CO_2 + 8\ H^+$, 0.17 V vs NHE at pH = 0)[49] and promote the separation of the photoformed holes from the valence band of the $K_2Ti_6O_{13}$ photocatalyst. In other words, the Rh cocatalyst would be bifunctional for both the oxidation and the reduction, and, as a result, the Rh cocatalyst was able to improve the whole photocatalytic activity. There are some reports that two kinds of cocatalysts for the oxidative and reductive reactions can cooperatively increase the entire photocatalytic activity; for example, $Pt/RuO_2/TiO_2$,[38] Pt/PdS/CdS,[16] $Pt/RuO_2/Zn_2GeO_4$,[50] Rh−Cr/Mn_3O_4/GaN-ZnO,[51] and $Rh/Ag_2S/Sm_2Ti_2S_2O_5$.[52] It is noted that the present simple photodeposition method can simultaneously generate both the rhodium metal nanoparticles promoting the reductive reaction and the rhodium oxide nanoparticles promoting the oxidative reaction on the $K_2Ti_6O_{13}$ photocatalyst.

3.4. Comparison with Other Semiconductor Photocatalysts. The influence of Pt and Rh cocatalysts was also examined for other semiconductor photocatalysts. They were loaded by the oxidative photodeposition method. The loading amount was optimized for each semiconductor sample as listed in Table 2. The Pt-loaded photocatalysts exhibited similar

Table 2. Hydrogen Production Rate in the PSRM over Various Photocatalysts Loaded with Pt or Rh Cocatalyst[a]

			optimum loading amount/wt %		hydrogen production rate/ μmol min^{-1}	
entry	photocatalyst	specific surface area[b]/ $m^2\ g^{-1}$	Pt	Rh	Pt-loaded sample	Rh-loaded sample
1	β-Ga_2O_3	11.7	0.05	0.05	0.65	0.52
2	$Na_2Ti_6O_{13}$	1.5	0.05	0.05	0.56	0.80
3	$K_2Ti_6O_{13}$	2.3	0.05	0.03	0.78	1.5
4	TiO_2	140	0.1	0.3	0.56	0.49

[a]Cocatalysts were loaded by the oxidative photodeposition method. [b]The values are for the photocatalyst without cocatalyst loading.

activity for PSRM to each other. In contrast, the Rh-loaded samples showed various activities, that is, the Rh-loaded β-Ga_2O_3 and TiO_2 photocatalysts showed slightly lower activities than the Pt-loaded samples did (Table 2, entries 1 and 4), while the Rh-loaded $Na_2Ti_6O_{13}$ and $K_2Ti_6O_{13}$ photocatalysts showed clearly higher activities than the Pt-loaded ones did (Table 2, entries 2 and 3).

From the edge shift in the Rh K-edge XANES (Figure 10A and 10B), it is obvious that all the Rh-loaded photocatalysts would contain rhodium oxide species to some extent. The edge shift in the spectrum of the Rh/TiO_2 photocatalyst was smaller than those for the other photocatalysts, showing that the amount of rhodium oxide species in the Rh/TiO_2 was smaller than those in the others.

In the Fourier transforms of the Rh K-edge EXAFS (Figure 10C), the peaks at 1.6 and 2.8 Å correspond to the Rh−O shell

dx.doi.org/10.1021/cs2006229 | ACS Catal. 2012, 2, 2126−2134

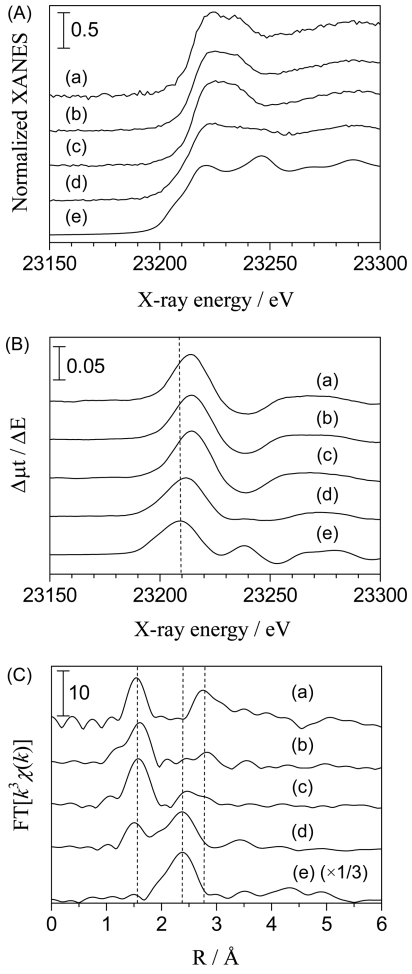

Figure 10. (A) Rh K-edge XANES, (B) derivative spectra of the XANES, and (C) Fourier transforms of Rh K-edge EXAFS for (a) Rh(0.1)/Ga_2O_3, (b) Rh(0.1)/$Na_2Ti_6O_{13}$, (c) Rh(0.1)/$K_2Ti_6O_{13}$, (d) Rh(0.1)/TiO_2 samples, and (e) rhodium foil. The Rh cocatalyst was loaded by the photodeposition method.

and the Rh−Rh shell in rhodium oxide, respectively, while the peak at 2.4 Å is the Rh−Rh shell in rhodium metal, as mentioned above. In the spectrum of the Rh/Ga_2O_3 sample, two peaks observed were assignable to the Rh−O shell and the Rh−Rh shell in rhodium oxide (Figure 10Ca), meaning that the Rh species on the Rh/Ga_2O_3 sample would be only composed of relatively large rhodium oxide particles. In the spectra of the Rh/$Na_2Ti_6O_{13}$ and Rh/$K_2Ti_6O_{13}$ samples, the three peaks were observed (Figure 10Cb and 10Cc), indicating that the Rh cocatalyst on these samples would be the mixture of rhodium metal and oxide particles. For the Rh/TiO_2 sample, the small peak assignable to the Rh−O shell in rhodium oxide and the large peak assignable to the Rh−Rh shell in rhodium metal were observed (Figure 10Cd), suggesting that the major rhodium species would be rhodium metal particles. These results confirmed that the high photocatalytic activity of the Rh-loaded $K_2Ti_6O_{13}$ and $Na_2Ti_6O_{13}$ photocatalysts would originate from the rhodium metal and oxide particles coexisting on them.

The intensities of the two peaks at 2.4 and 2.8 Å reflected the relative particle sizes of the rhodium metal and oxide particles among these samples, respectively. The intensity of the peak at 2.4 Å for the metal species decreased in the following order, TiO_2 > $K_2Ti_6O_{13}$ > $Na_2Ti_6O_{13}$ > Ga_2O_3, and that of the peak at 2.8 Å for the oxide species increased in the following order, TiO_2 < $K_2Ti_6O_{13}$ < $Na_2Ti_6O_{13}$ < Ga_2O_3. These orders were clearly correlated with the order of their bandgaps: 3.2 eV for anatase-TiO_2, 3.4 eV for $K_2Ti_6O_{13}$, 3.5 eV for $Na_2Ti_6O_{13}$, and 4.6 eV for β-Ga_2O_3 (Supporting Information, Figure S1). That is, the ratio of the metallic moiety to the oxidized moiety decreased with increasing bandgap of the semiconductors.

During the formation of the Rh cocatalyst by the present photodeposition method in the presence of dissolved oxygen, the photoexcited electrons would be competitively consumed for not only the reduction of the rhodium ions but also the activation of the oxygen (Figure 11). The activated oxygen

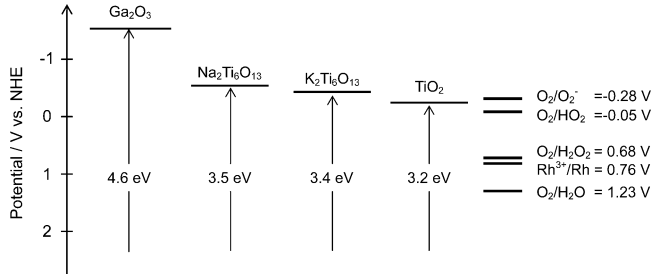

Figure 11. Potential of the conduction band edge and the measured bandgap in the semiconductors, and the reduction potentials of oxygen[21] and rhodium ion.[53] The potentials of the conduction band edge in Ga_2O_3 and TiO_2 were reported in the literature.[54] Those of $Na_2Ti_6O_{13}$ and $K_2Ti_6O_{13}$ were estimated from their bandgap values, assuming that the each valence band edge was about 2.94 eV.[46].

species would combine with rhodium cation to form rhodium oxide species. The good relationship observed between the order of the conduction band position and the ratio of oxidized moiety suggests that the highly negative potential of the conduction band edge would further enhance the activation of oxygen, which would oxidize the rhodium species to form rhodium oxide particles. Since the alkaline titanate photocatalysts have the moderate conduction band potential, the mixture of the metallic and oxidized rhodium cocatalysts would be fabricated. In the case of the Pt cocatalyst loading, the coexistence of oxygen could not much influence the oxidation state of the Pt cocatalyst, since Pt is more easily reduced (Pt^{2+} + $2e^-$ → Pt, 1.19 V vs NHE)[53] and not easily oxidized. At present, we could not rule out other possibilities that the acid−base property or the low specific surface area of the alkaline titanate photocatalysts might also influence the ratio of the rhodium metal to oxide species. Further experiments are now carried out to clarify this point.

4. CONCLUSION

Photocatalytic steam reforming of methane was examined over metal-loaded alkaline titanate photocatalysts. The activity of the photocatalysts was much influenced by the loading method as well as the kind and the amount of the metal cocatalyst. The highest activity was obtained over the Rh(0.03 wt %)-loaded $K_2Ti_6O_{13}$ photocatalysts prepared by the oxidative photodeposition method. Over the highly active Rh-loaded photocatalysts, small Rh metal particles and large Rh oxide ones coexisted, and they cooperatively promoted the reductive and oxidative reactions, respectively, to increase the entire photocatalytic activity. Thus, the present Rh cocatalyst can be recognized as a bifunctional cocatalyst.

Although photodeposition method is a popular way to deposit metal cocatalyst nanoparticles on the semiconductor

dx.doi.org/10.1021/cs2006229 | ACS Catal. 2012, 2, 2126−2134

photocatalyst, the relationship between the preparation condition and their structure has not been fully understood. The present study provided the new insights that the oxidation state of metal cocatalyst and the photocatalytic activity were much influenced by both the properties of semiconductor and the preparation conditions. Further examination of the photodeposition method should lead to the development of more active photocatalysts.

■ ASSOCIATED CONTENT

Supporting Information

Further detail is given in Figure S1. This material is available free of charge via the Internet at http://pubs.acs.org.

■ AUTHOR INFORMATION

Corresponding Author

*E-mail: yoshidah@apchem.nagoya-u.ac.jp.

Funding

This work was partially supported by a Grant-in-Aid for Scientific Research (C) (No. 2156799) and a Grant-in-Aid for Scientific Research on Priority Area "Strong Photon Molecule Coupling Fields" No. 470 (No. 21020017) from the Ministry of Education, Culture, Sports, Science and Technology (MEXT) of the Japanese Government. K.S. was supported by a Grant-in-Aid for Nagoya University Global COE programs (Elucidation and Design of Materials and Molecular Functions).

Notes

The authors declare no competing financial interest.

■ ACKNOWLEDGMENTS

We thank Professor S. Muto (Nagoya University) for providing the opportunity to take the TEM images. The X-ray absorption experiments of the Rh-loaded samples were performed under the approval of the Photon Factory Program Advisory Committee (Proposal No. 2008G510, 2010G149, and 2011G575).

■ REFERENCES

(1) Shimura, K.; Yoshida, H. *Energy Environ. Sci.* **2011**, *4*, 2467−2481.
(2) Yoshida, H.; Kato, S.; Hirao, K.; Nishimoto, J.; Hattori, T. *Chem. Lett.* **2007**, *36*, 430−431.
(3) Yoshida, H.; Hirao, K.; Nishimoto, J.; Shimura, K.; Kato, S.; Itoh, H.; Hattori, T. *J. Phys. Chem. C* **2008**, *112*, 5542−5551.
(4) Shimura, K.; Kato, S.; Yoshida, T.; Itoh, H.; Hattori, T.; Yoshida, H. *J. Phys. Chem. C* **2010**, *114*, 3493−3503.
(5) Shimura, K.; Yoshida, T.; Yoshida, H. *J. Phys. Chem. C* **2010**, *114*, 11466−11474.
(6) Shimura, K.; Yoshida, H. *Energy Environ. Sci.* **2010**, *3*, 615−617.
(7) Shimura, K.; Miyanaga, H.; Yoshida, H. *Stud. Surf. Sci. Catal.* **2010**, *175*, 85−92.
(8) Shimura, K.; Maeda, K.; Yoshida, H. *J. Phys. Chem. C* **2011**, *115*, 9041−9047.
(9) Shimura, K.; Yoshida, H. *Phys. Chem. Chem. Phys.* **2012**, *14*, 2678−2684.
(10) Domen, K.; Kudo, A.; Onishi, T.; Kosugi, N.; Kuroda, H. *J. Phys. Chem.* **1986**, *90*, 292−295.
(11) Kudo, A.; Tanaka, A.; Domen, K.; Maruya, K.; Aika, K.; Ohishi, T. *J. Catal.* **1988**, *111*, 67−76.
(12) Kato, H.; Asakura, K.; Kudo, A. *J. Am. Chem. Soc.* **2003**, *125*, 3082−3089.
(13) Inoue, Y. *Energy Environ. Sci.* **2009**, *2*, 364−386.
(14) Maeda, K.; Teramura, K.; Lu, D. L.; Takata, T.; Saito, N.; Inoue, Y.; Domen, K. *Nature* **2006**, *440*, 295.
(15) Maeda, K.; Domen, K. *J. Phys. Chem. Lett.* **2010**, *1*, 2655−2661.
(16) Yan, H. J.; Yang, J. H.; Ma, G. J.; Wu, G. P.; Zong, X.; Lei, Z. B.; Shi, J. Y.; Li, C. *J. Catal.* **2009**, *266*, 165−168.
(17) Zong, X.; Wu, G. P.; Yan, H. J.; Ma, G. J.; Shi, J. Y.; Wen, F. Y.; Wang, L.; Li, C. *J. Phys. Chem. C* **2010**, *114*, 1963−1968.
(18) Zhang, W.; Wang, Y. B.; Wang, Z.; Zhong, Z. Y.; Xu, R. *Chem. Commun.* **2010**, *46*, 7631−7633.
(19) Hara, M.; Nunoshige, J.; Takata, T.; Kondo, J. N.; Domen, K. *Chem. Commun.* **2003**, 3000−3001.
(20) Liu, M. Y.; You, W. S.; Lei, Z. B.; Zhou, G. H.; Yang, J. J.; Wu, G. P.; Ma, G. J.; Luan, G. Y.; Takata, T.; Hara, M.; Domen, K.; Li, C. *Chem. Commun.* **2004**, 2192−2193.
(21) Abe, R.; Takami, H.; Murakami, N.; Ohtani, B. *J. Am. Chem. Soc.* **2008**, *130*, 7780−7781.
(22) Arai, T.; Horiguchi, M.; Yanagida, M.; Gunji, T.; Sugihara, H.; Sayama, K. *Chem. Commun.* **2008**, 5565−5567.
(23) Kraeutler, B.; Bard, A. J. *J. Am. Chem. Soc.* **1978**, *100*, 5985−5992.
(24) Mills, A.; Le Hunte, S. *J. Photochem. Photobiol. A* **1997**, *108*, 1−35.
(25) Yoshida, H.; Yuzawa, H.; Aoki, M.; Otake, K.; Itoh, H.; Hattori, T. *Chem. Commun.* **2008**, 4634−4636.
(26) Yoshida, H. *Environmentally benign photocatalysts: Applications of titanium oxide-based materials*; Anpo, M., Kamat, P. V., Eds.; Springer: New York, 2010; Chapter 27, pp 647−669.
(27) Shiraishi, Y.; Sugano, Y.; Tanaka, S.; Hirai, T. *Angew. Chem., Int. Ed.* **2010**, *49*, 1656−1660.
(28) Yuzawa, H.; Yoshida, H. *Chem. Commun.* **2010**, *46*, 8854−8856.
(29) Yuzawa, H.; Mori, T.; Itoh, H.; Yoshida, H. *J. Phys. Chem. C* **2012**, *116*, 4126−4136.
(30) Inoue, Y.; Kubokawa, T.; Sato, K. *J. Phys. Chem.* **1991**, *95*, 4059−4063.
(31) Sayama, K.; Arakawa, H. *J. Photochem. Photobiol., A* **1994**, *77*, 243−247.
(32) Shimura, K.; Kawai, H.; Yoshida, T.; Yoshida, H. *Chem. Commun.* **2011**, *47*, 8958−8960.
(33) Nomura, M.; Koike, Y.; Sato, M.; Koyama, A.; Inada., Y.; Asakura, K. *AIP Conf. Proc.* **2007**, *882*, 896−898.
(34) Lytle, F. W.; Greegor, R. B.; Sandstorm, D. R.; Marques, E. C.; Wong, J.; Spiro, C. L.; Huffman, G. P.; Huggins, F. E. *Nucl. Instrum. Methods* **1984**, *226*, 542−548.
(35) Mckale, A. G.; Veal, B. W.; Paulikas, A. P.; Chan, S. K.; Knapp, G. S. *J. Am. Chem. Soc.* **1988**, *110*, 3763−3768.
(36) Bamwenda, G. R.; Tsubota, S.; Nakamura, T.; Haruta, M. *J. Photochem. Photobiol., A* **1995**, *89*, 177−189.
(37) Kalyanasundaram, K.; Gratzel, M. *Angew. Chem., Int. Ed. Engl.* **1979**, *18*, 701−702.
(38) Kawai, T.; Sakata, T. *Nature* **1980**, *286*, 474−476.
(39) Duonghong, D.; Borgarello, E.; Gratzel, M. *J. Am. Chem. Soc.* **1981**, *103*, 4685−4690.
(40) Hara, M.; Waraksa, C. C.; Lean, J. T.; Lewis, B. A.; Mallouk, T. E. *J. Phys. Chem. A* **2000**, *104*, 5275−5280.
(41) Kasahara, A.; Nukumizu, K.; Hitoki, G.; Takata, T.; Kondo, J. N.; Hara, M.; Kobayashi, H.; Domen, K. *J. Phys. Chem. A* **2002**, *106*, 6750−6753.
(42) Iwase, A.; Kato, H.; Kudo, A. *Chem. Lett.* **2005**, *34*, 946−947.
(43) Harriman, A.; Pickering, I. J.; Thomas, J. M.; Christensen, P. A. *J. Chem. Soc., Faraday Trans.* **1988**, *84*, 2795−2806.
(44) Hrussanova, A.; Guerrini, E.; Trasatti, S. *J. Electroanal. Chem.* **2004**, *564*, 151−157.
(45) Koffyberg, F. P. *J. Phys. Chem. Solids* **1992**, *53*, 1285−1288.
(46) Scaife, D. E. *Solar Energy* **1980**, *25*, 41−54.
(47) Nieuwenhuys, B. E.; Bouwman, R.; Sachtler, W. M. H. *Thin Solid Films* **1974**, *21*, 51−58. Michaelson, H. B. *J. Appl. Phys.* **1977**, *48*, 4729−4733.
(48) Wood, D. M. *Phys. Rev. Lett.* **1981**, *46*, 749.
(49) Indrakanti, P. V.; Kubicki, J. D.; Schobert, H. H. *Energy Environ. Sci.* **2009**, *2*, 745−758.

(50) Ma, B.; Wen, F.; Jiang, H.; Yang, J.; Ying, P.; Li, C. *Catal. Lett.* **2010**, *134*, 78−86.
(51) Maeda, K.; Xiong, A.; Yoshinaga, T.; Ikeda, T.; Sakamoto, N.; Hisatomi, T.; Takashima, M.; Lu, D.; Kanehara, M.; Setoyama, T.; Teranishi, T.; Domen, K. *Angew. Chem., Int. Ed.* **2010**, *49*, 4096−4099.
(52) Zhang, F.; Maeda, K.; Takata, T.; Domen, K. *Chem. Commun.* **2010**, *46*, 7313−7315.
(53) The Chemical Society of Japan, *Kagakubinran Kisohen*, 3rd ed.; Maruzen: Tokyo, Japan, 1984.
(54) Xu, Y.; Schoonen, M. A. A. *Am. Mineral.* **2000**, *85*, 543−556.